An Automated Common Algorithm for Planetary Boundary Layer Retrievals Using Aerosol Lidars in Support of the U.S. EPA Photochemical Assessment Monitoring Stations Program

Vanessa Caicedo,[a,b] Ruben Delgado,[a,b] Ricardo Sakai,[c] Travis Knepp,[d,e] David Williams,[f] Kevin Cavender,[g] Barry Lefer,[h] and James Szykman[e,f]

[a] *Joint Center of Earth Systems Technology, Baltimore, Maryland;* [b] *University of Maryland, Baltimore County, Baltimore, Maryland;* [c] *Howard University, Washington, D.C.;* [d] *Science Systems and Applications, Inc., Hampton, Virginia;* [e] *National Aeronautics and Space Administration Langley Research Center, Hampton, Virginia;* [f] *Office of Research and Development, U.S. Environmental Protection Agency, Research Triangle Park, North Carolina;* [g] *Office of Air Quality Planning and Standards, U.S. Environmental Protection Agency, Research Triangle Park, North Carolina;* [h] *National Aeronautics and Space Administration Headquarters, Washington, D.C.*

ABSTRACT: A unique automated planetary boundary layer (PBL) retrieval algorithm is proposed as a common cross-platform method for use with commercially available ceilometers for implementation under the redesigned U.S. Environmental Protection Agency Photochemical Assessment Monitoring Stations program. This algorithm addresses instrument signal quality and screens for precipitation and cloud layers before the implementation of the retrieval method using the Haar wavelet covariance transform. Layer attribution for the PBL height is supported with the use of continuation and time-tracking parameters, and uncertainties are calculated for individual PBL height retrievals. Commercial ceilometer retrievals are tested against radiosonde PBL height and cloud-base height during morning and late-afternoon transition times, critical to air quality model prediction and when retrieval algorithms struggle to identify PBL heights. A total of 58 radiosonde profiles were used, and retrievals for nocturnal stable layers, residual layers, and mixing layers were assessed. Overall good agreement was found for all comparisons, with one system showing limitations for the cases of nighttime surface stable layers and daytime mixing layer. It is recommended that nighttime shallow stable-layer retrievals be performed with a recommended minimum height or with additional verification. Retrievals of residual-layer heights and mixing-layer comparisons revealed overall good correlations with radiosonde heights (square of correlation coefficients r^2 ranging from 0.89 to 0.96, and bias ranging from approximately -131 to $+63$ m for the residual layer and r^2 from 0.88 to 0.97 and bias from -119 to $+101$ m for the mixing layer).

KEYWORDS: Boundary layer; Algorithms; Lidars/Lidar observations; Remote sensing; Air quality

1. Introduction

The planetary boundary layer (PBL) is the lowest layer in the atmosphere directly influenced by Earth's surface (Stull 1988). The diurnal evolution of the PBL typically consists of the convective mixing layer (ML) during the daytime and the residual layer (RL) during nighttime containing the remains of the daytime ML above the near-surface nocturnal stable layer (SL) (Stull 1988). Here we refer to these layers individually as SL, RL, and ML or collectively as the PBL. The PBL depth defines the vertical extent and distribution of pollutants making it a vital parameter in meteorological, climatological, air pollution, and numerical model simulation studies. The complex diurnal evolution of the PBL for air pollution is best understood through continuous monitoring. As such, remote sensing instruments such as aerosol lidars (e.g., ceilometers), Doppler wind lidars, Raman lidars, and radars lend themselves well for continuous monitoring and have been extensively explored in recent years to provide monitoring of the PBL in the time scales needed for climate, meteorological, and air quality studies. Technology advancements have made aerosol lidar and ceilometers a cost-effective alternative to autonomously monitor the PBL. For this reason, various remote sensing networks are being established throughout the world creating a need for a robust and automated method to derive PBL heights (PBLHs) from large heterogeneous datasets. Here we assess the application of a common algorithm for use within a heterogeneous lidar (ceilometer) network such as the U.S. Environmental Protection Agency (EPA) Photochemical Assessment Monitoring Stations (PAMS) program.

Aerosol backscatter retrieval methods perform under the assumption that the ML contains relatively homogeneous concentrations of aerosols due to convective and turbulent mixing. These aerosols are capped by the clean free troposphere above the ML, creating a significant negative gradient in aerosol at this transition point, and therefore aerosol backscatter gradients. This negative gradient (i.e., top of the aerosol layer) is then attributed to the ML height (MLH) (Steyn et al. 1999). In the case of a stratified PBL, the search of aerosol backscatter gradients that correspond to an SL, RL, or ML must be carefully considered. This creates a significant challenge for times of rapid PBL growth or decay such as the morning transition of the SL into the convective ML, or in the late afternoon when the PBL often becomes stratified as a result of decreasing solar radiation leading to multiple aerosol layers and therefore multiple aerosol gradients with decreasing vertical mixing (Stull 1988). Because of this

Corresponding author: Vanessa Caicedo, caicedo.vanessa@gmail.com

dynamic and complex nature of the PBL, the development of automated PBLH retrievals that can be used under various PBL conditions is crucial.

To estimate PBLH retrievals from aerosol backscatter, several mathematical methods have been tested and implemented. These include methods such as the quantitative identification of a maximum gradient in an aerosol backscatter profile (e.g., Schäfer et al. 2004; de Bruine et al. 2017; Kotthaus and Grimmond 2018a,b) or the use of variance in aerosol backscatter signals to identify the MLH corresponding to the largest peak in aerosol backscatter variance (Toledo et al. 2014; Caicedo et al. 2017). These two methods, however, often fail because of sensitivity to ceilometer noise particularly in higher altitudes (Caicedo et al. 2017; Kotthaus and Grimmond 2018a,b). Other methods include the idealized-profile fitting methods (e.g., Steyn et al. 1999; Eresmaa et al. 2006) and utilizing wavelet transforms to accentuate significant aerosol backscatter gradients in aerosol backscatter profiles (e.g., Cohn and Angevine 2000; Davis et al. 2000; Brooks 2003; de Haij et al. 2006; Baars et al. 2008; Scarino et al. 2014; Uzan et al. 2016). Further, several studies merge strengths from various methods into retrieval algorithms such as Lammert and Bösenberg (2006), Martucci et al. (2007, 2010), Morille et al. (2007), Di Giuseppe et al. (2012), Pal et al. (2013), Hicks et al. (2015), Geiß (2016), Geiß et al. (2017), Peng et al. (2017), Poltera et al. (2017), and Hicks et al. (2019). However, under stratified PBLs, all methods remain challenged by aerosol layer attribution which can be address through the implementation of tracking techniques (e.g., Lewis et al. 2013; Geiß 2016; Poltera et al. 2017; Bonin et al. 2018).

Some studies have explored supplementing aerosol backscatter data with additional measurements for the detection of the PBLH (Pal et al. 2013; Hicks et al. 2015); however, additional measurements may not be continuously collected or available at all sites. Further, available commercial software requires a manual selection from the user such as the Vaisala BL-View software packages for Vaisala ceilometers (Münkel and Roininen 2010). This software has been implemented with varying results in studies such as Haman et al. (2012, 2014), Lotteraner and Piringer (2016), Münkel et al. (2007), Tang et al. (2016), Knepp et al. (2017), and Wagner and Schäfer (2017). The disagreement between results is likely due to the subjective selection of the PBLH by the user which can introduce additional bias between results.

Another factor for increasing uncertainties in aerosol derived PBLHs is the varying design among different manufacturers of commercial ceilometers and their derivation techniques for attenuated aerosol backscatter. These must be taken into account before the implementation of PBL retrieval techniques such as those performed by Haeffelin et al. (2012), Vande Hey et al. (2012), Madonna et al. (2015), Hervo et al. (2016), Kotthaus et al. (2016), Poltera et al. (2017), and Madonna et al. (2018).

Although several efforts to test and validate aerosol PBLH retrieval methods using a diverse range of instrumentation have been performed (e.g., Münkel et al. 2007; Emeis et al. 2008b; Haeffelin et al. 2012; Hicks et al. 2015; Caicedo et al. 2017) varying results were found without arriving at a preferred method. Most importantly, studies observe differences between a thermodynamically and aerosol derived PBLHs, as aerosols can overshoot into higher altitudes and therefore display overestimations when compared to thermodynamic PBLHs (McElroy and Smith 1991; Seibert et al. 2000; Wang et al. 2012; Dang et al. 2019). As a possible data source for model validation, aerosol backscatter retrievals must be accurate and reliable for the use of the numerical modeling community. Biavati et al. (2015) and Pal et al. (2013) suggest that aerosol derived PBLH methods should report retrieval uncertainties; however, no current retrieval method or algorithm known to the authors is able to give uncertainties to individual aerosol backscatter derived PBLHs or insight into the performance of the retrieval algorithms. As retrieval methods define the PBLH as the absolute height where the maximum negative gradient or maximum aerosol backscatter gradient is present, no uncertainties of the PBLH are reported. Some methods report uncertainties by averaging PBLH retrievals over time; however, these are not representative of the PBLH retrieval method itself. More recently, Biavati et al. (2015) proposed a method for arriving at error estimations by calculating uncertainties through vertical profiles. Although these uncertainties can give indications of instrumental signal errors, they do not give insight into the retrieval algorithm's performance.

To undertake the development for an automated and robust PBLH retrieval algorithm for long-term heterogeneous datasets, this study expands on the Haar wavelet covariance transform method. The proposed algorithm addresses both instrument specific issues and the inherent PBLH detection limitations described above. Ceilometer signal quality is addressed by implementing signal corrections for noise, artifacts, and overlap issues in measured aerosol backscatter profiles (section 3a). The PBLH retrieval algorithm then applies a range of dilations of the wavelet transform, calculates the mean of the transforms which in turn improves the detection of weak aerosol gradients in conditions with low aerosol content and low altitudes (Caicedo et al. 2017), and allows for the ability to calculate uncertainties in the PBLH retrieval. The application of a continuation and time-tracking parameter is used to aid in layer attribution and reduce misidentification of aerosol layers during transition times. Cloud identification using wavelet method independent of commercial cloud retrievals is implemented for the first time as strong cloud signals can decrease correlations between thermodynamic and aerosol-derived PBLHs (Caicedo et al. 2017). The proposed method results in a unique automated algorithm that addresses instrumental signal quality, multiple layers in the PBL diurnal evolution, derive cloud layers using the same PBL retrieval method, routinely screens for precipitation, and continuity in signals, while reporting retrieval uncertainties. The algorithm is discussed in detail in section 3 and its performance across various instrumentation is tested against radiosonde PBLHs in section 4, in order to assess its application on heterogeneous ground-based remote sensing networks.

2. Data and instrumentation

a. Photochemical Assessment Monitoring Stations network

The EPA PAMS network implemented as part of the 1990 Clean Air Act Amendments required enhanced monitoring of ozone, ozone precursors, and meteorological factors for evaluating, tracking the progress of, and informing ozone control
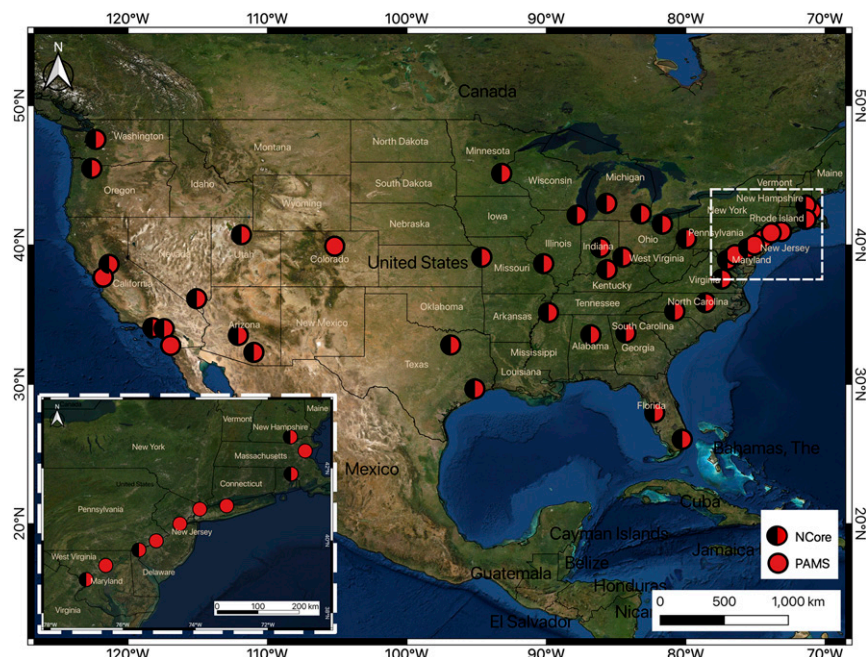
FIG. 1. Map of the continental United States showing the locations of the PAMS (red circles) network sites with a requirement for hourly MLH. PAMS collocated with NCore sites (black and red circles) are also shown.

strategies. Driven by the changing nature of ozone concentrations across the nation, the EPA finalized a 2015 redesign of PAMS with a focus on improved precursor measurements, characterization of upper air meteorology and/or pollution measurements, and PBL profiling measurements with the MLH as a required parameter at PAMS (EPA 2019). Through the use of commercially available remote sensing instrumentation, with the primary instrumentation being aerosol backscatter ceilometers, the PAMS network will create a geographically distributed network of tropospheric profiling measurements including the detection of aerosol layers and the MLH. Instrumentation will be deployed at 43 sites (Fig. 1) covering the continental United States with many of the PAMS sites collocated with measurements from EPA National Core Network (NCore), a multipollutant network primarily focused on measurements for particles, resulting in a combined suite of measurements to better understand urban air quality issues. Data from the network will advance the spatiotemporal coverage of much needed PBL monitoring for air pollution studies including the validation of operational model simulations and support the monitoring of air pollution events such as exceptional events of dust and smoke transport. A centralized data processing effort is currently being established for adequate reporting of MLHs, enhanced retrieval algorithms, standardized software and calibration procedures, and to provide an efficient infrastructure to uniformly gather, verify, and distribute the data for near-real-time implementation and reporting (EPA 2019).

b. ACES

The measurements used in this study were taken as part of the Ad-Hoc Ceilometer Evaluation Study (ACES); a collaboration between the EPA Office of Research and Development and the University of Maryland, Baltimore County (UMBC), to help guide the implementation of hourly MLHs for the EPA's PAMS program. Because the hourly MLH requirement is not limited to a particular profiling system, ACES was an independent study to evaluate available commercial ceilometers as the mostly likely instrumentation to be used in PAMS. ACES goals included the evaluation of the attenuated backscatter from commercially available ceilometers, the commercial software and firmware, the assessment of the daytime ML height determination with a focus on transition periods (i.e., morning ML growth and afternoon ML decay), and the development of a unified PBL retrieval method using aerosol backscatter signals. Four commercial ceilometers (Lufft CHM15k, Vaisala CL51, Vaisala CL31, and Campbell SkyVUE PRO) were collocated at the UMBC campus in Catonsville, Maryland (39.2544°N, 76.7095°W), between 1 and 15 December 2016. The campaign was focused on the winter months because this would display the most challenging conditions for PBLH retrievals as cooler surface temperatures, reduced daylight hours, and minimum solar radiation lead to stable and stratified PBL conditions in addition to relatively lower aerosol content during winter periods. Date, time, and ceilometer type for data used to evaluate the proposed algorithm are displayed in Fig. 2.

c. Radiosonde data and retrievals

Four–five balloonborne radiosonde launches were performed during measurement days typically at about 1200, 1400, 1600, 2100, and 2300 UTC (0700, 0900, 1100, 1600, and 1800 EST) to capture transition periods. A total of 58 launches were performed. Because of numerous definitions of the PBLH
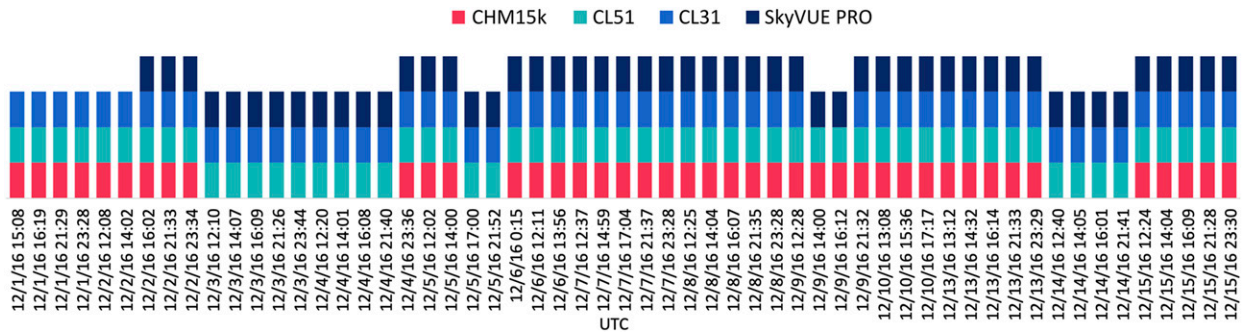
FIG. 2. Date and time of each radiosonde launch and associated ceilometer data availability for ACES.

(Stull 1988; Garratt 1992) multiple techniques have been proposed to estimate the PBLH from radiosonde thermodynamic, wind, and humidity profiles. Among the most common techniques are the parcel method (e.g., Holzworth 1964; Seibert et al. 2000), bulk Richardson (e.g., Troen and Mahrt 1986; Sørensen et al. 1998), humidity gradient methods (e.g., Seidel et al. 2010; Hicks et al. 2015), and potential temperature techniques (e.g., Heffter 1980; Liu and Liang 2010). Yet under neutral and unstable conditions, parcel methods tend to result in under estimations of the PBLH and require surface temperature measurements (Delle Monache et al. 2004; Seidel et al. 2010), while humidity-based methods generally yield higher PBLH estimates and can be influenced by cloud gradients incorrectly identified as the PBLH (Seidel et al. 2010). The bulk Richardson method requires reliable wind data, can be highly influenced by improper surface parameterizations, and tends to fail under stable conditions (Seibert et al. 2000). The automated potential temperature method proposed by Heffter (1980) and later expanded by Marsik et al. (1995) is used in this study as an objective measurement less subject to moisture and stability limitations than the humidity-based and parcel methods. This method searches for a critical inversion (critical stable layer) surpassing a potential temperature lapse rate threshold indicating the top of the ML. The Heffter (1980) method has been found to have difficulties in diverse environments (i.e., coastal, mountainous, and continental sites) due to inappropriate threshold definitions and has been found to systematically overestimate the PBLH (Marsik et al. 1995; Piringer et al. 1998; Delle Monache et al. 2004; Snyder and Strawbridge 2004). For this reason, the Heffter method is applied similarly to that in Delle Monache et al. (2004), Snyder and Strawbridge (2004), and Sivaraman et al. (2013) which modifies threshold definitions and adds a stable PBL detection technique. Under stable conditions, the height of the lowest inversion or the height of the low-level jet (whichever is lowest) is identified as the PBLH. During unstable/neutral conditions, the PBLH is identified as the height within a potential temperature inversion which exceeds the critical lapse rate threshold and exceeds a second threshold defined as the potential temperature difference between the top and bottom of the inversion layer. Here the critical lapse rate of $0.005 \, \mathrm{K\,m^{-1}}$ and a potential temperature difference threshold of $2 \, \mathrm{K}$ are used as these were shown to work best in coastal environments (Delle Monache et al. 2004). A second verification is performed during stable conditions as

the Heffter method can fail to identify shallow nocturnal surface inversions. Under these conditions, the SL is defined as the height above which temperature decreases with height (Stull 1988; Bradley et al. 1993; Seidel et al. 2010). A cloud-topped ML is defined as the base of the cloud layer. Each radiosonde PBLH retrieved by the Heffter method is categorized into an SL, RL, ML, or cloud-topped ML following Stull (1988) for comparison with ceilometer retrievals.

In addition to the validation of PBLH retrievals, cloud-base heights (CBH) retrievals using the Haar wavelet method are evaluated against sonde CBHs. Following Zhang et al. (2010), CBHs are determined using relative humidity (RH) to identify the presence of moist layers and/or clouds. First, a moist layer is identified when RH is above 84% with at least a 3% difference in RH from below the moist layer to the base of the layer, and from the top of the layer to the air above. Clouds layers are identified if the maximum RH of the moist layer is above 87%.

d. Ceilometer instrumentation

The instruments used in this study are the Lufft CHM15k, Vaisala CL51, Vaisala CL31, and Campbell Scientific SkyVUE PRO ceilometers. Table 1 lists basic information for each ceilometer. The vertical range of full overlap is listed, as incomplete lidar signals due to optical overlap can limit ceilometer retrievals in regions below full overlap. Adequate corrections for the regions are key for near-surface aerosol layer detection in particular for instruments with increasing range of complete overlap. Figure 2 displays data availability for all ceilometers and corrections to ceilometer signals are discussed in section 3a. Communication errors or power outages at the times of radiosonde launches were experienced by the CHM15k, CL31, and SkyVUE PRO. The CHM15k in particular, experienced data gaps due to temporary power surges which led to a system shutdown and unsuccessful restart.

3. PBL retrieval algorithm

The automated PBLH retrieval algorithm proposed here only uses aerosol backscatter signal without the need for additional measurements. For this reason, the algorithm first addresses aerosol backscatter signal quality and applies corrections and signal smoothing to aerosol backscatter profiles. The algorithm then screens signals for precipitation and clouds, followed by the application of the Haar wavelet transform on

TABLE 1. Description of ceilometers used in this study.

	CHM15k	CL51	CL31	SkyVUE PRO
Wavelength	1064 nm	910 nm	905 nm	905 nm
Pulse	8 μJ	3 μJ	1.2 μJ	4.8 μJ
Pulse length	1 ns	110 ns	110 ns	100 ns
Vertical range	15 km	15 km	7.7 km	10 km
Design and configuration	Biaxial lens; photon counting detector	Single lens; analog detection	Single lens; analog detection	Single split lens; analog detection
Approximate complete optical overlap	~1700 m	~550 m	~70 m	~300–400 m; Vande Hey et al. (2012) and
Overlap > 90%	~700 m	~220 m	~55 m	Madonna et al. (2018)
Reported temporal resolution	37 s	36 s	15 s	10–30 s
Reported vertical resolution	15 m	10 m	10 m	5 m

aerosol backscatter profiles. The following sections detail the comprehensive algorithm.

All ceilometer data are binned according to ceilometer reported temporal resolution (Table 1) to account for any gaps in data. For example, each daily file for the Vaisala CL31 ceilometer should contain 5760 profiles with each bin increasing from 0000 to 2359 UTC every 15 s. If no measurement was reported, the bin will remain empty. All vertical values are reported in meters above ground level (AGL).

a. Signal correction

A heterogeneous aerosol lidar network includes instruments with design and performance differences and requires different preprocessing of the data for correction and signal smoothing before the application of the PBLH retrieval algorithm. For further studies and long-term operational networks, using individual aerosol backscatter profiles calibration procedures should be explored such as those described in O'Connor et al. (2004), Wiegner and Geiß (2012), Baars et al. (2016), and Hopkin et al. (2019). The following section details documented issues associated with ceilometers listed in Table 1 involving individual ceilometer reported signals (RS), and the corresponding corrected return signals (CRS). The minimum reliable height Z_{min} for each instrument is defined by taking into account individual instrument signal characteristics. Note that restricting retrievals above Z_{min} may, in turn, remove signals from shallow layers and hence limit the identification of shallow PBLHs. Aerosol backscatter in the nearest 500 m and daily average profile for each ceilometer is presented in Fig. 3. Differences in signals displayed in Fig. 3 are in part due to different laser wavelengths of each system.

Recent studies show that ambient temperature changes affect the CHM15k photodetector which in turn distorts the overlap function but can be corrected using an automated technique proposed by Hervo et al. (2016) which applies a correction function to the known manufacturer's overlap correction function. The data used here are corrected using the Hervo et al. (2016) method before the application of the retrieval algorithm. CHM15k overlap artifacts in near-surfaces ranges required Z_{min} to be defined at 200 m (Fig. 3a).

The CL51 (Fig. 3b) displays an artifact at ~40 m as seen in the data, and therefore, Z_{min} for the CL51 is conservatively defined at 110 m. The CL31 (Fig. 3c) displays a well-documented artifact at 40–50 m (Sokół et al. 2014; Kotthaus et al. 2016; Caicedo et al. 2017)

in aerosol backscatter profiles when using specific firmware versions (Kotthaus et al. 2016). Increasing vertical moving averages (higher averaging in higher altitudes) are applied to CL31 profiles beginning at 15 m in the lowest altitudes and increasing to 130 m at maximum ranges similarly applied by Emeis et al. (2008a,b). Hence, Z_{min} for the CL31 is set to 110 m. This also serves to reduce any effects from optical overlap as the CL31 full overlap is reached at approximately 70 m (Münkel et al. 2007). The CL31 used in this study follows Kotthaus et al. (2016) recommendations for firmware version, settings, and hardware configurations, yet no background correction is applied as it will not impact PBL signals or PBL retrievals. Another source of errors was recently discussed by Wiegner et al. (2019) for ceilometers operating in the 900–910 nm range such as the CL31, CL51 and SkyVUE PRO. As Wiegner et al. (2019) shows, this interference from water vapor absorption affects absolute aerosol backscatter values but does not affect the shape of the profiles. Because the PBLH retrieval algorithm does not depend on absolute values but rather on aerosol profile shape (significant decrease with height in aerosol backscatter), a water vapor correction is not applied.

The SkyVUE PRO data displayed irregular artifacts in aerosol backscatter profiles. Wiegner et al. (2019) found larges differences in aerosol backscatter and deterioration in signals above the mixing layer from two SkyVUE PRO ceilometers. Madonna et al. (2015) found electronic distortion in signals in the upper troposphere and signal artifacts likely due to the effect of environmental temperature particularly during warm periods which affect temperature control or temperature correction errors, on the SkyVUE PRO hardware. The irregular artifacts found in the data (Fig. 4a) were improved using a ninth-order, one-dimensional (time) mean filtering (Mather 1987) applied to individual vertical profiles (Fig. 4b). Overlap and artifacts in near-surfaces ranges required Z_{min} to be defined as 120 m (Fig. 3d). Due to high noise in signals, vertical smoothing is applied to SkyVUE PRO data similarly to those applied to the CL31.

b. Precipitation screening

After the signal corrections detailed in section 3a are applied daily, CRS profiles are then averaged into 10-min aerosol backscatter profile bins ($\overline{CRS}$). $\overline{CRS}$ profiles are flagged for precipitation before the application of the Haar wavelet
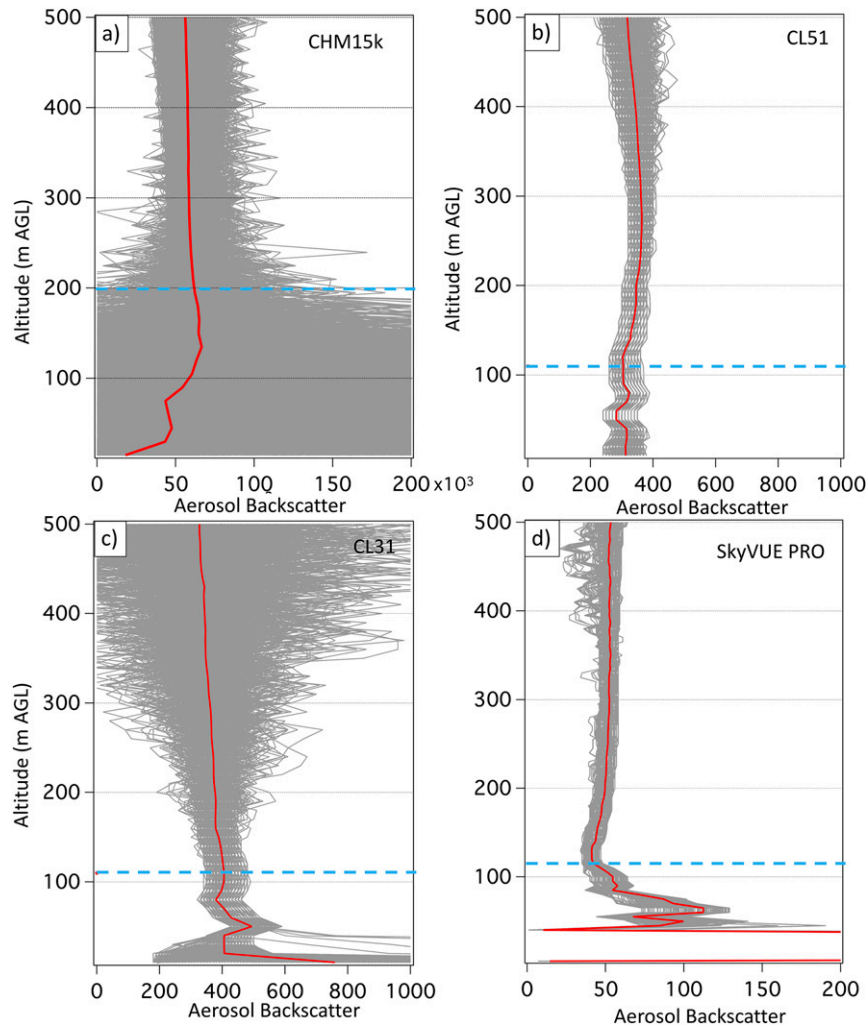
FIG. 3. Examples of aerosol backscatter in the nearest 500 m reported by (a) CHM15k, (b) CL51, (c) CL31 and (d) SkyVUE PRO for 10 Dec 2016. Horizontal blue dashed lines indicate Z_{min} defined for each instrument. Daily average profile for each instrument is displayed as red solid lines.

transform PBLH retrieval method. To identify precipitation periods, the algorithm searches for continuous regions of high backscatter surpassing an absolute threshold. Threshold values are defined from CRS signals; however, thresholds can also be defined for signals before commercial corrections as precipitation signals will present distinctively high values. These thresholds are defined as $2000 \times 10^{-9} \, \mathrm{m^{-1} \, s^{-1}}$ for CL31, CL51, and SkyVUE PRO, and $400\,000 \, \mathrm{m^{-1} \, s^{-1}}$ for the CHM15k as only precipitation signals should yield such large values. To rule out cloud signals, precipitation areas must begin near the surface and extend upward for a minimum of 200 m. If precipitation is identified in a $\overline{\mathrm{CRS}}$ profile, a PBL retrieval will be automatically invalid; however, cloud-layer heights can still be identified.

c. Haar wavelet transform parameter selection

The Haar wavelet transform method was selected for the implementation of the aerosol lidar PBLH retrieval algorithm.

Caicedo et al. (2017) tested various methods for PBLH retrievals using aerosol backscatter profiles and found the Haar wavelet method to be the most reliable and robust. Here we use multiple Haar wavelet dilations to identify aerosol backscatter gradients and retrieve PBLHs (Cohn and Angevine 2000; Davis et al. 2000; Brooks 2003; Baars et al. 2008; Compton et al. 2013; Uzan et al. 2016). The covariance transform $w_f(a, b)$ of the Haar wavelet function $h[(z - b)/a]$ is defined as

$$ w_f(a, b) = a^{-1} \int_{\mathrm{CRS_{min}}}^{\mathrm{CRS_{max}}} f(z) h\left(\frac{z - b}{a}\right) dz, $$

where a is the dilation factor (vertical extent) of the Haar function, b is the center of the Haar wavelet function, $\mathrm{CRS_{min}}$ and $\mathrm{CRS_{max}}$ are the lower and upper ranges of ceilometer signals (vertical ranges in Table 1), and $f(z)$ is the $\overline{\mathrm{CRS}}$ profile
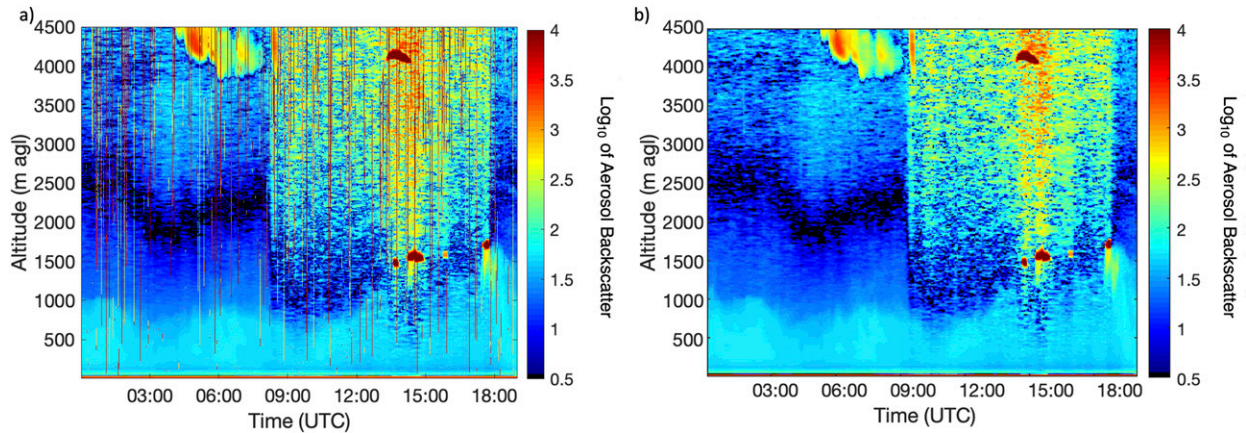
FIG. 4. The 10 Dec 2016 raw aerosol backscatter reported by (a) SkyVUE PRO and (b) corrected backscatter using the ninth-order, one-dimensional filter.

as a function of altitude z. The covariance transform is applied to $\overline{CRS}$ (Fig. 5a) from CRS_{min} to CRS_{max} with incremental dilations ($a = a_0$–a_i; selection of values is discussed below) until the maximum dilation factor a_i is reached (e.g., in Fig. 5b). The determination of the dilation factors or vertical extent of the Haar function a defines the number of local minimums in w_f (a, b) or the covariance wavelet transform coefficient (CWTC) local minimums. Larger a values create fewer large local minima, and lower dilation values create numerous CWTC local minima at the heights of aerosol gradients in the measured profiles. The algorithm uses the mean of all resulting CWTC profiles ($\overline{CWTC}$) and detects local minimums in the $\overline{CWTC}$ profiles for PBL identification (Fig. 5c). The detection of the CWTC minimum is constrained to the previously defined Z_{min} height for each ceilometer and to a defined upper height limit. Additionally, a regional maximum PBLH (Z_{max})

is defined based on previous studies and/or literature. For this study region, $Z_{max} = 3000$ m (Lewis et al. 2013).

The proper definition of parameters for the Haar wavelet transform is key for the correct identification of the PBLH. The Haar wavelet method was seen to decrease in performance under a stratified PBL (Caicedo et al. 2017) such of the nocturnal stratified PBL, or the stratified decoupling of the ML in the afternoon hours. To improve the performance under these conditions, the dilation factor range from a_0 to a_i and height detection limits (hl) are defined following Stull (1988) stages of the ML evolution using local sunrise (SR) and sunset (SS) times. Stull (1988) defined three stages of ML evolution: stratification of the PBL and formation of shallow ML, rapid ML growth, and deep convective ML periods (Fig. 6). Using these stages, the algorithm performs retrievals based on defined parameters for each stage. For the study region during
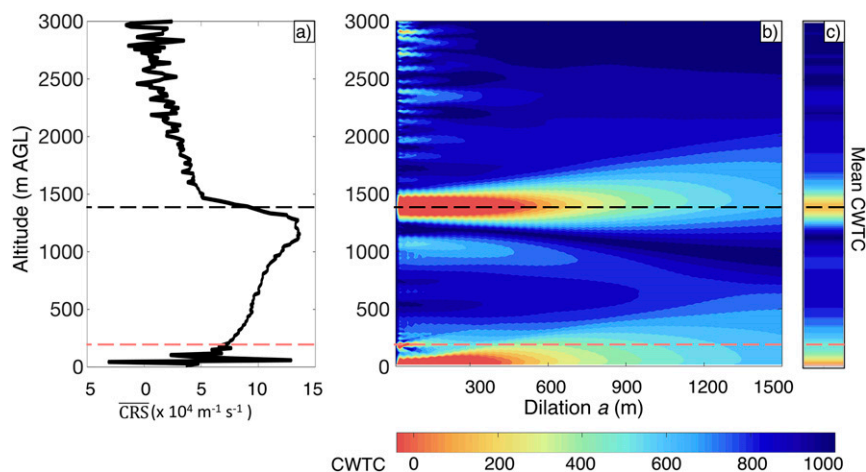

FIG. 5. (a) CHM15k $\overline{CRS}$ profile, and (b) the corresponding CWTC coefficients calculated with increasing dilations from $a_0 = 15$ m to $a_i = 1500$ m, and (c) the resulting mean $\overline{CWTC}$. Note that CWTC profiles are displayed up to Z_{max} (3000 m), but Haar wavelet transform is applied to the entire $\overline{CRS}$ profile (from CRS_{min} to CRS_{max}). The horizontal red dashed line indicates Z_{min}, and the horizontal black dashed line signifies the identified PBLH.
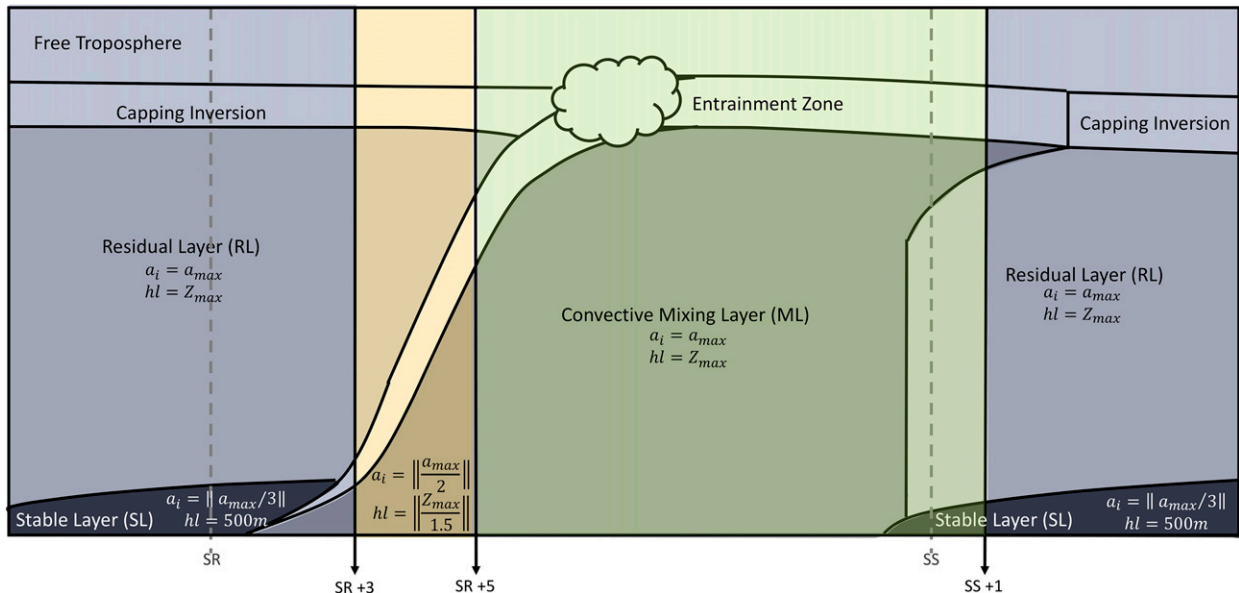
FIG. 6. PBL evolution modified from Stull (1988). Shading indicates the temporal division of settings for the Haar wavelet algorithm.

this time SR and SS were at approximately 1200 UTC (0700 EST) and 2200 UTC (1700 EST), respectively.

For all of the three ML stages, the minimum dilation factor a_0 is defined as the first reported measurement height of each ceilometer [a_0(CL31) = 10 m; a_0(CL51) = 10 m; a_0(CHM15k) = 15 m; a_0(SkyVUE) = 5 m] while a_{max} is carefully defined for each instrument model through user testing focused on optimal a_i definition for well-mixed PBL signals. The first algorithm stage begins 1 h after sunset (SS + 1) and ends 3 h after SR (SR + 3) as shown in the blue regions in Fig. 6. This period typically consists of a stratified PBL with the initial growth of the shallow ML near the surface, and the RL containing the remains of the previous days ML above the SL. The RL typically displays heights that are similar to those of the previous day's ML, whereas both the SL and developing ML are expected at shallow heights near the surface. After SR, the ML grows slowly due to the strong SL (nocturnal inversion) capping the developing ML (Stull 1988). For measurements taken during this first stage, two separate retrievals are used in order to detect shallow SLs and MLs, and deeper RLs. For RL retrievals, the Haar wavelet transforms is defined with height limit hl = Z_{max}, and $a_i = a_{max}$ as RLs are often associated with the largest gradients in aerosol backscatter profiles. SL retrievals settings are defined with hl = 500 m and, $a_{i(SL)} = a_{max}/3$. Both hl_{SL} and $a_{i(SL)}$ are reduced for SL and ML retrievals for this stage in order to identify near surface aerosol layers below 500 m using small a values that could identify weak aerosol backscatter gradients in a stratified PBL (Caicedo et al. 2017). The value hl = 500 m is used because early-morning and nocturnal stable layers are expected below this height limit (Haman et al. 2012; Seidel et al. 2012; Liu and Liang 2010; Rappenglück et al. 2008), and $a_{i(SL)} = a_{max}/3$ is decreased from a_{max} in order to identify more aerosol layers under increasingly stratified conditions.

Once the ML first surpasses the strong SL inversion it experiences rapid growth rates hence, the second stage continues for the next two hours when the rapid growth of the ML is expected, reaching the RL top by late morning (Stull 1988). This period has parameters hl = $Z_{max}/1.5$ and, $a_i = a_{max}/2$, which were increased from the previous nocturnal period but do not reach maximum defined parameters. This is done to allow the identification of multiple negative gradients during the growth of the ML while strong signals from the RL may still be present. During this time, the two separate retrievals from the first detection stage (for shallow SLs and MLs, and deep RLs) are discontinued as RL and ML signals were often found in close proximities during the study period.

The final stage is defined with hl = Z_{max} and, $a_i = a_{max}$ because a well-mixed ML is expected to display the strongest local minimum in the CWTC profile. This period begins 5 h after SR and ends 1 h after sunset. As Stull (1988) states, rising thermals cease about 30 min before SS; therefore, the algorithm allows for an extra 30 min for distinct aerosol layering formation.

d. Cloud-layer screening and identification

$\overline{CWTC}$ profiles are evaluated for cloud-layer signals before the identification of a PBLH. The identification of cloud signals uses the $\overline{CWTC}$ profiles because the cloud base will be transformed into a significantly strong local maximum while the cloud top will be displayed as a strong local minimum (Fig. 7). $\overline{CWTC}$ cloud detection uses profiles generated using a_0–a_{max} as strong cloud signals are easily identified and transform into large local maximum and minimums.

To screen $\overline{CWTC}$ profiles for cloud signals, a cloud threshold is first defined ($2000 \times 10^{-9}\,\mathrm{m^{-1}\,s^{-1}}$ for CL31, CL51, and SkyVUE PRO, and $400\,000\,\mathrm{m^{-1}\,s^{-1}}$ for the CHM15k) based on Caicedo et al. (2017) and van der Kamp and McKendry (2010).
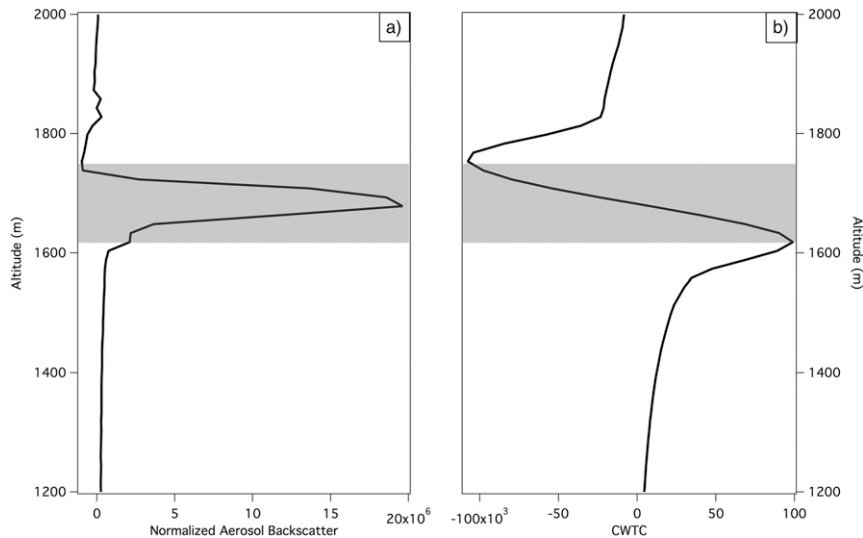
FIG. 7. (a) CHM15k $\overline{CRS}$ profile for 2030 UTC 13 Dec 2016, and (b) its corresponding $\overline{CWTC}$ profile. Shaded regions enclose the cloud layer at the identified cloud-base and cloud-top heights.

If the $\overline{CWTC}$ profile surpasses the defined cloud thresholds, the profile is flagged as containing cloud signals, and the identification of up to three cloud layers is performed as it is unlikely that ceilometer lasers will penetrate more than three clouds layers without significant signal attenuation. Figure 7a shows a CHM15k $\overline{CRS}$ with a cloud layer at about 1000 m. The corresponding $\overline{CWTC}$ transform is displayed in Fig. 7b. The Haar wavelet algorithm identifies the $\overline{CWTC}$ local maximum as the cloud-base height and the local minimum as the cloud-top height (CTH) for up to three cloud layers in a single $\overline{CWTC}$ profile. The presence of drizzle or virga below the cloud layer should be carefully considered as this may introduce bias to CBH due to signal below the cloud mistakenly identified as the CBH.

e. PBLH identification

Once the Haar wavelet transforms with predefined parameters (section 3c) are applied, the resulting $\overline{CWTC}$ profiles are used to identify the PBLH. The algorithm stores the strongest local minimums in individual $\overline{CWTC}$ profiles and sorts them according to strength. The largest local minimum is the first guess PBLH. As previously mentioned, aerosol layering and PBL stratification limits the retrieval of a single PBL using aerosol backscatter profiles hence, a continuation parameter is implemented to prevent sharp changes in the retrievals as the PBL depth should not change in short time periods (Stull 1988). The first guess PBLH is tested for continuity by comparing the height of this local minimum to the previously identified PBLH. If the local minimum is not within 200 m of the previously defined PBLH, the second strongest minima are tested for continuity in the same manner. If none of the four largest local minima are within the 200-m threshold, a PBLH is not reported. The identification of SLs, RLs, and MLs all undergo the continuation parameter. The first retrieval for a daily file is also required to meet the continuation check using the

previous day's retrievals. Here we use the previous defined 10-min PBLH as the comparison point therefore limiting the validation to the past 10 min. If no prior data are available, the first guess PBLH is used. This constraint was applied to aid the robust reporting of automated PBL retrievals but could be increased to a larger time interval if needed.

f. PBLH uncertainty calculation

The Haar wavelet transform using a range of dilations (a_0–a_{max}) allows for the calculation of uncertainty in the retrieved PBLH. Local minima for each CWTC generated from a_0 to a_{max} is saved and compared with the final retrieved PBL from $\overline{CWTC}$ profiles described in sections 3c and 3e by calculating the standard deviation of CWTC generated from a_0 to a_{max} from the $\overline{CWTC}$ PBLH. This gives insight into the vertical structure of the PBL and the overall performance of the algorithm. If multiple layers are present, dilations at lower ranges will create local minima at multiple layers, while larger dilations will identify the largest local min, and therefore, large departures from the mean will be calculated. The calculation of standard deviation also serves as an additional tool to optimize Haar wavelet transform parameters. These values can be used to assess the parameters used and arrive at the best parameters possible that will keep standard deviations in acceptable ranges (<200 m). For instance, if a_0–a_{max} is constrained to relatively low values, significantly high standard deviations may be reported as multiple gradients will be detected when using small dilation values (section 3c). As such, the 200-m range can be adjusted to account for deeper convective PBLs or instances of strong stratification.

g. Quality checks

The standard deviation is used to further verify retrievals by excluding retrievals with standard deviations above 200 m. PBLH retrievals identified at times when precipitation was

TABLE 2. Results from ceilometer and radiosonde comparisons divided by classified stable layer (SL), mixing layer (ML), residual layer (RL), and cloud-base heights (CBH). Results for each ceilometer comparison include the number of comparison points available (No. points), linear regression correlation coefficient (r^2), slope of linear regression line, offset of linear regression line, bias, mean radiosonde heights, and mean ceilometer height.

		SL	ML	RL	CBH
No. points	CHM15k	3	24	5	11
	CL51	7	33	8	17
	CL31	7	26	6	17
	SkyVUE PRO	6	18	4	12
	Radiosonde	7	37	11	17
r^2	CHM15k	0.37	0.88	0.96	0.99
	CL51	0.03	0.97	0.95	0.98
	CL31	0.01	0.91	0.92	0.95
	SkyVUE PRO	0.33	0.91	0.89	0.97
Slope	CHM15k	−1.47	0.95	1.28	0.95
	CL51	−0.32	0.88	1.16	0.97
	CL31	0.27	0.94	1.87	0.87
	SkyVUE PRO	1.13	0.97	1.73	0.97
Offset (m)	CHM15k	464.1	75.6	−232.0	80.3
	CL51	316.4	130.2	−145.5	13.1
	CL31	240.6	43.4	−785.3	110.3
	SkyVUE PRO	304.9	157.7	−662.7	69.2
Bias (m)	CHM15k	206.4	93.0	63.3	135.5
	CL51	173.2	21.2	22.3	−27.5
	CL31	161.7	−118.9	−131.0	−88.1
	SkyVUE PRO	327.6	24.1	2.3	39.0
Mean radiosonde (m)		108.3	108.3	1003.9	967.7
Mean ceilometer (m)	CHM15k	314.7	1096.9	1031.0	1660.6
	CL51	281.4	1025.2	990.0	1497.7
	CL31	270.0	885.0	836.7	1437.1
	SkyVUE PRO	435.8	1028.1	970.0	1564.2

identified are automatically removed. Cloud signals can create difficulty for the Haar wavelet algorithm as these signals tend to either attenuate aerosol backscatter above the cloud layer or create enhanced signals immediately below the cloud base. If a CBH is identified within 300 m of the identified PBLH, the PBLH is removed. Note that under a cloud-topped ML, the PBLH = CBH, and therefore, only a CBH is reported. The final 10-min retrievals are reported with a standard deviation after all quality checks are performed in order to arrive at the most robust and automated outputs. In addition to PBL retrievals with reported standard deviations, aerosol backscatter profiles used in conjunction with retrievals provide further context needed to understand PBL vertical structure and aerosol layering

4. PBLH retrieval validation results

To validate and assess the performance of the PBL retrieval algorithm, the radiosondes PBLHs were classified as SL, RL, ML, or cloud-topped ML (cML) as described in section 2c and displayed in Table 2. Note that CBH and cML grouped together in the CBH results. Although early-morning launches were performed, not all 1200 UTC launches showed a surface inversion, which resulted in the Heffter method overestimating or not detecting the SL. In these cases, a second verification was performed to define the SL (section 2c). If an SL was not identified, only RL heights were used for validation.

A two-sided, paired sample t test is used to define the statistical significance of the bias. The null hypothesis is defined as

unbiased aerosol derived heights when compared with radiosonde heights. It was not rejected when the calculated t test value t was within ± 2 and the p value was greater than 0.05% or 95% confidence.

First the percentage of initial PBL retrievals identified by the algorithm was calculated for all available radiosonde PBL comparisons. This initial comparison used a PBLH as discussed in section 3e, which included postprocessing for signal correction, precipitation screening, continuity parameters, and cloud-layer screening (sections 3a–3d). This resulted in 93%, 96%, 98%, and 95% of PBLHs identified for CHM15k, CL51, CL31, and SkyVUE PRO data, respectively. For CBH comparisons, all ceilometers found 100% CBHs for all available data due to the strong cloud signals that are easily identified in all ceilometer data.

The final quality check of uncertainty applied a standard deviation test (section 3f) to the above-mentioned initial retrievals. This resulted in 14%, 9%, 25%, and 40% removal of initial PBLH retrievals for CHM15k, CL51, CL31, and SkyVUE PRO, respectively. Higher uncertainties were observed in the CL31 and SkyVUE PRO instruments likely due to higher noise and signal artifacts (section 3a). Figure 8 shows removed PBL retrievals and their standard deviations in lighter colors for each ceilometer. Although some of the retrievals removed correlated well with radiosonde PBLHs, instances where multiple significant aerosol gradients were found are removed for reliable PBL reporting. Recognizing
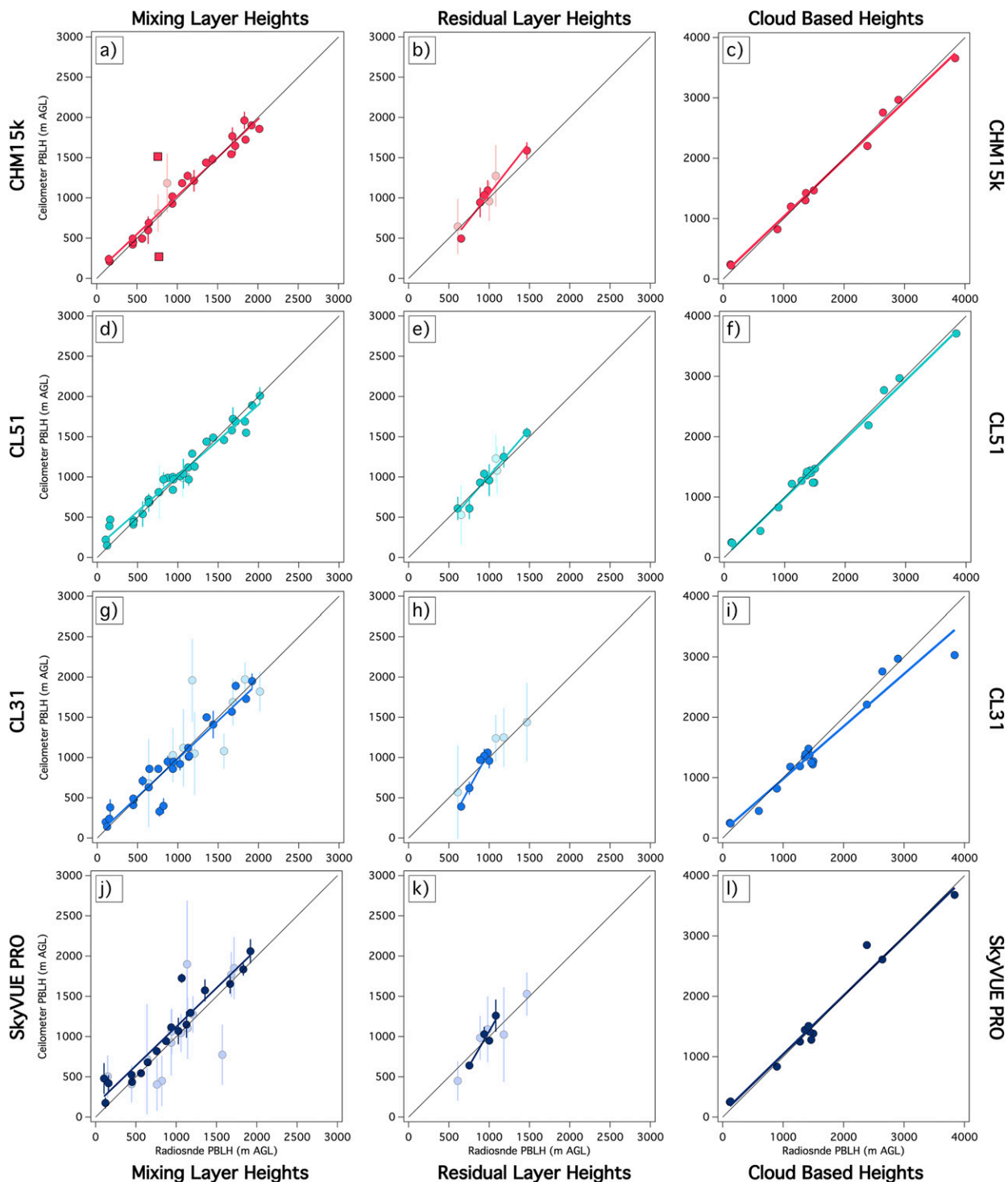
FIG. 8. Linear regression results for retrievals classified as (left) ML, (center) RL, and (right) CBHs for (a)–(c) CHM15k, (d)–(f) CL51, (g)–(i) CL31, and (j)–(l) SkyVUE PRO ceilometers. Error bars display calculated algorithm uncertainties. Lighter-colored symbols represent disqualified retrievals removed because of uncertainties surpassing the quality check limit of 200 m.

these instances are key as future users of long-term automated networks should be able to use consistent retrievals that have been screened for instances when retrievals may be unreliable (i.e., PBL stratification).

Table 2 displays correlations between radiosonde PBLHs and final ceilometer derived heights. Linear regression correlation coefficient squared r^2, the slope and y intercept for linear regression, mean radiosonde height, mean ceilometer, and mean bias calculated as the difference between ceilometer and radiosonde are used to describe the magnitude of the difference between benchmark radiosonde and derived ceilometer results. Radiosonde PBLHs were compared with a 10-min bin including the radiosonde launch time (e.g., 1234 launch time was compared with the 10-min bin calculated from 1230 to 1240 UTC). The resulting number of comparison points are also indicated in Table 2 to account for instances in which no PBLH was found by the automated algorithm.

The statistical test performed rejected the SL comparisons for all ceilometers and that of the SkyVUE PRO ML results. These SL comparisons displayed the least amount of validation points, the lowest correlation to radiosonde heights, and overall overestimated SL heights from ceilometers. The overestimation of SL heights is clearly due to the use of the Z_{min} which confines the retrieval of an aerosol gradient to above Z_{min} preventing unreliable near surface artifacts and/or optical overlap. Therefore, an SL with a depth larger than Z_{min} can only be identified. As previously mentioned, ACES was conducted in December at a time of low aerosol loading and colder temperatures when only three radiosonde launches found an SL $> Z_{min}$. Detection of the SL may improve in warmer months with less stable and faster convective growth from greater solar heating of the surface or in areas with higher aerosol loading. Data interruptions associated with the CHM15k ceilometer during the detection of the SL limited the number of comparisons to three data points. Although, at times ceilometer retrievals identified layers at heights corresponding to shallow inversions, it is suggested that ceilometer retrieved SL heights be used only above the recommended minimum height (Z_{min}) and/or using other auxiliary thermodynamic data. Additional validation studies focused on the SL may help define Z_{min} more precisely and improve SL detection. Further, improvements to optical overlap can also improve these retrievals.

The CL51 ceilometer performed best in comparison to the radiosonde PBLHs. RL comparisons revealed significantly higher correlations than SL as the RL altitudes are higher and not as close to the Z_{min}. No SL retrievals were disqualified from the comparison after the standard deviation check, and a larger amount of RL retrievals were removed in comparison to MLs results. This final quality check removed 38%, 27%, 40% and 55% of reported RL heights from CHM15k, CL51, CL31, and SkyVUE PRO, respectively. This result indicates that identification of the SL and RL during nighttime hours for a heterogeneous ceilometer ground-based network maybe be limited during times with multiple aerosol layering. The comparisons showed slight overestimations of the RL height for all ceilometers except the CL31 which showed some underestimated outliers in the comparisons (Figs. 8b,e,h,k). RL comparisons after the final quality check for the CHM15k and

TABLE 3. Overall results of all comparison (48 radiosondes' PBLH) performed including number of ceilometer retrievals available, linear regression correlation coefficient (r^2), slope of linear regression, offset of linear regression, bias, and root-mean square error.

	CHM15k	CL51	CL31	SkyVUE PRO
No. points	29	41	32	22
r^2	0.88	0.96	0.90	0.90
Slope	0.96	0.90	0.96	0.97
Offset (m)	64.65	116.75	27.39	134.52
Bias (m)	−89.91	−22.66	119.69	−21.88
RMSE (m)	194.05	94.33	156.83	168.88

SkyVUE PRO were limited to 5 and 4 points, respectively; therefore, results should be carefully considered.

ML comparisons contained the most comparison points and displayed good agreement with radiosonde MLHs (Figs. 8a,d,g,j). The final quality check for uncertainties removed 8%, 6%, 26%, and 44% of ML retrievals for the CHM15k, CL51, CL31, and SkyVUE PRO, respectively. Instrument noise in the CL31 and the SkyVUE PRO retrievals is the likely cause for the large percent of flagged retrievals in these two instruments. This resulted in the SkyVUE PRO comparisons failing the paired sample t test, although the final comparisons show good agreement to radiosonde PBLHs (Fig. 8j). All ceilometers showed positive bias (ranging from approximately 21 to 101 m) except for the CL31. This is likely the result of the two outliers in the CL31 ML comparison (Fig. 8g), which resulted from low aerosol loading and algorithm identification of small noise gradients. Aerosols overshooting thermal gradients (McElroy and Smith 1991; Seibert et al. 2000) is a typical reason for positive bias. The two CHM15k outliers shown in Fig. 8a (displayed as squares) revealed possible effects in laser wavelengths. The two radiosonde profiles detected a PBLH that also corresponds to the identification a moist layer (>84% RH) as calculated with the Zhang et al. (2010) method but was not ultimately identified as a cloud layer. It is likely that the ceilometers in the 900 nm wavelength range were more sensitive to the presence of moisture in the profile and therefore detected a negative gradient corresponding to the radiosonde PBLH, while the CHM15k (1064 nm) did not present a significant aerosol backscatter gradient at this height and therefore attributed the PBLH to another aerosol gradient found.

CBH comparisons showed the best agreement of all comparisons, and therefore, the Haar wavelet method is deemed reliable for CBH retrievals. The CL31 retrieval showed a slightly lower CBH retrieval for one instance where aerosol backscatter signals were detected at a slightly lower height than that of the radiosonde CBH. This may be due to any moisture below the cloud height (i.e., drizzle/virga) but more likely due to vertical smoothing of signals for the CL31 as other ceilometers did not display the same underestimation. The CHM15k showed the largest bias calculated of 101.6 m; however, it should be noted that due to data interruptions (Fig. 2), only nine comparisons were possible. In contrast, CL31, CL51 and SkyVUE PRO comparisons contained 12–17 points.

Overall statistics for PBLH retrievals (excluding SL heights because of statistical test failure) are shown in Table 3 for a
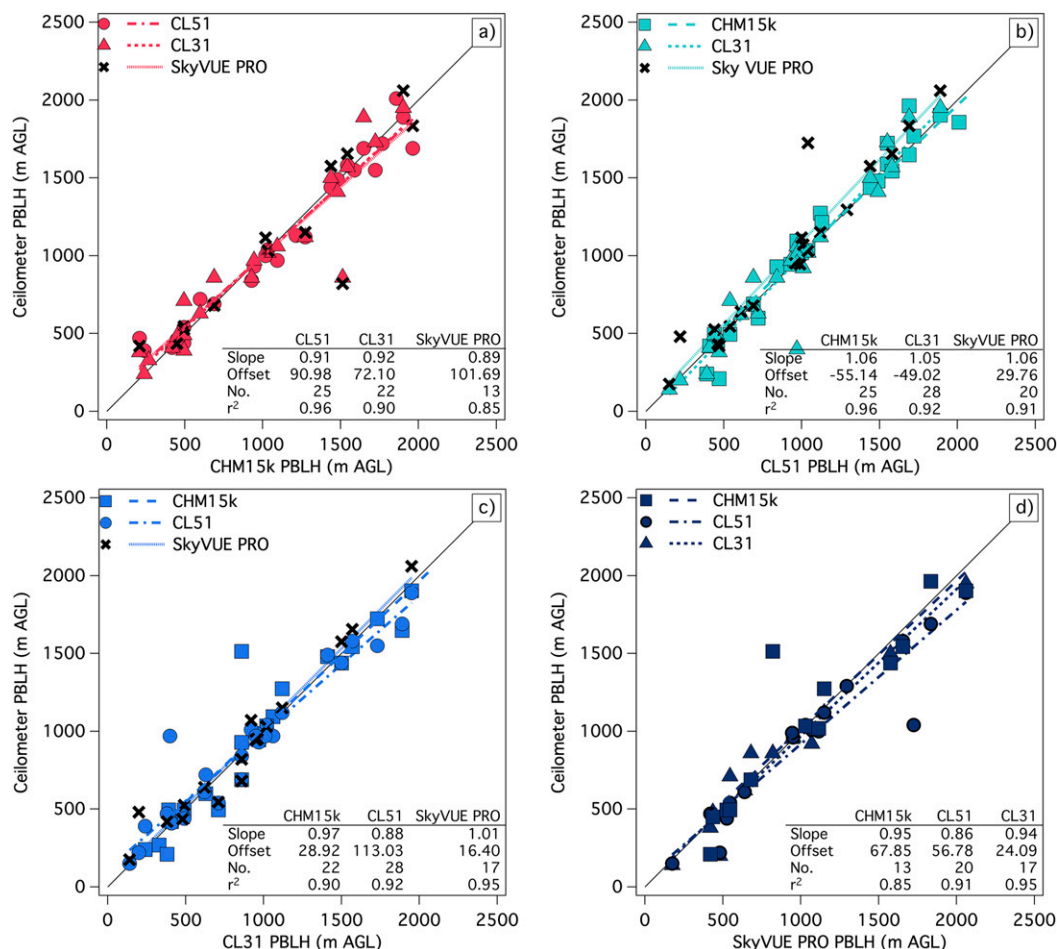
FIG. 9. Linear regression of ceilometer retrieval intercomparison for (a) CHM15k, (b) CL51, (c) CL31, and (d) SkyVUE PRO ceilometers. Results of all linear regressions are listed, including the linear regression slope, offset, number of points used (No.), and correlation coefficient (r^2). Ceilometer comparisons use squares and large dashed lines for CHM15k, circles and dash–dotted lines for CL51, triangles and small dashed lines for CL31, and crosses and dotted lines for SkyVUE PRO comparisons.

total of 48 comparisons. Bias was found to be below 200 m for all ceilometer except for the SL SkyVUE PRO comparison. The SkyVUE PRO ceilometer displayed the lowest correlations and consistently higher errors in comparisons to radiosonde PBLHs. This was attributed to noise in SkyVUE PRO data that was not improved by the smoothing and correction tools described in section 3a.

Comparison between ceilometers is displayed in Fig. 9. All comparisons show good agreement between ceilometers, with the least agreement when comparing SkyVUE PRO ceilometer retrievals. The CHM15k showed correlations with typically slightly higher PBLHs than those found by the other ceilometers. The effect of differences in wavelengths should be further investigated in these cases.

Figure 10 shows retrievals for 13 December 2016, a day on which five radiosonde launches were performed. Figure 10 displays $\overline{\text{CWTC}}$ aerosol backscatter profiles and corresponding automated retrievals (black circles) from 1200 to 0000 UTC. From 1200 to 1500 UTC the algorithm is performing under the

previously described stage 1 when two retrievals are attempted in order to find SL and RL signals. Figures 10a–c show the nocturnal retrievals (i.e., nocturnal settings search for a deep RL and/or a shallow SL) found a single aerosol gradient ∼500 m corresponding to the height of an unstable/neutral layer retrieved using two radiosonde profiles. However, the SkyVUE PRO ceilometer RL retrievals detected higher altitude signals due to signal noise/artifacts (Fig. 10d). After 1500 UTC and before 2300 UTC, the retrieval performs the second stage described in section 3c, which searches for a single MLH. During this time, upper cloud layers were detected above the MLH. The radiosondes at ∼1600 UTC and ∼2130 UTC reveal good agreement for both MLH and CBH retrievals for all ceilometers except the SkyVUE PRO which displayed retrievals with uncertainties >200 m and were therefore not reported. The last launch on this day at ∼2330 UTC fell into the first stage of the automated algorithm which again searches for two aerosol layers. All ceilometers retrievals found one of the two retrievals at the
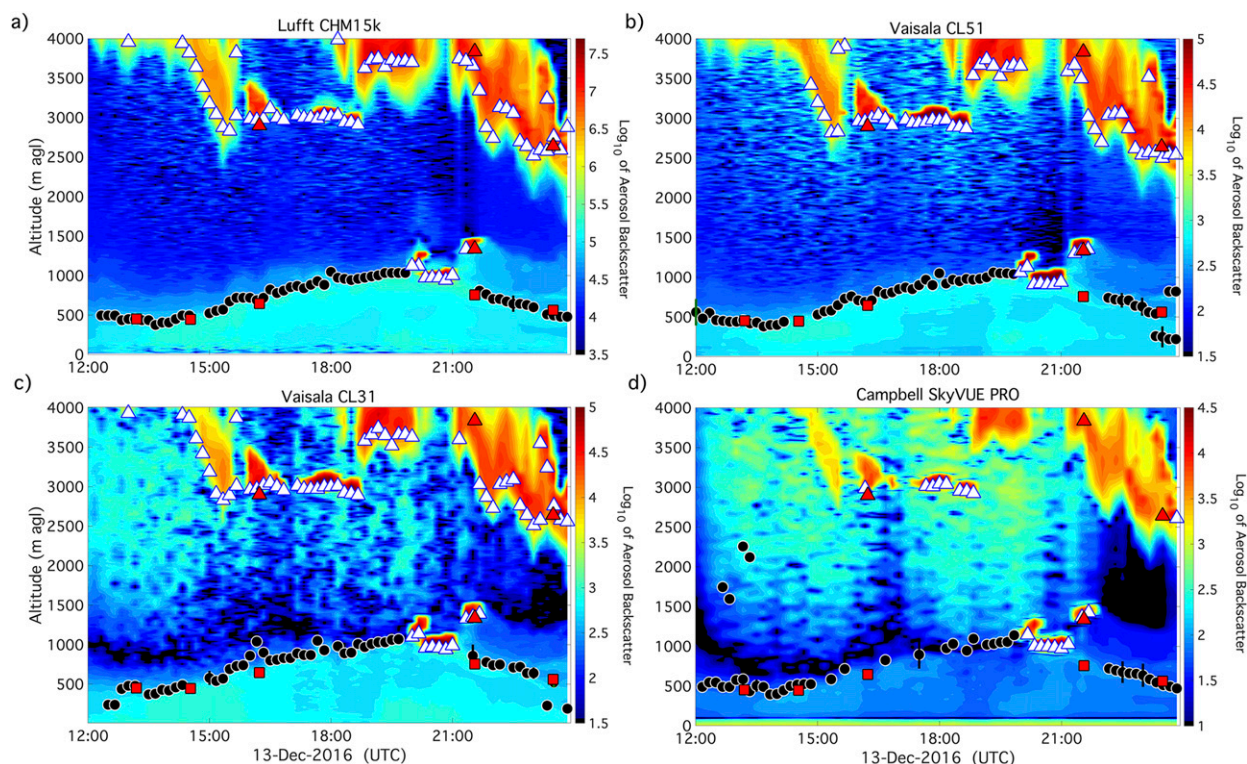
FIG. 10. 13 Dec 2016 $\overline{CWTC}$ profiles from (a) CHM15k, (b) CL51, (c) CL31, and (d) SkyVUE PRO ceilometers. PBLH retrievals from the automated algorithm are displayed with black circles, and CBH retrievals are displayed as white triangles. Radiosonde heights for PBLHs and CBH are displayed as red squares and red triangles, respectively. Error bars display 10-min retrieval uncertainties every 30 min for display clarity purposes, although uncertainties are calculated with every 10-min retrieval.

height of the radiosonde height. In this case, the afternoon transition period was adequately captured by the automated retrieval specially during times when multiple strong gradients were present at ~500 and ~800 m. Both of these layers were also seen as unstable layers and potential temperature inversions in the radiosonde profile. Figure 10d also shows significantly reduced CBH retrievals for the SkyVUE PRO. Although extensive testing for optimal combinations of signal corrections, signal smoothing, and Haar wavelet dilation values were tested, no combination increased the output for the SkyVUE PRO ceilometer.

5. Summary and discussion

Aerosol-backscatter-derived planetary boundary layer heights from an automated retrieval algorithm using the Haar wavelet covariance transform method are assessed. The algorithm was developed for the common application to varying aerosol lidar/ceilometer instrumentation for future heterogeneous PBL monitoring networks, such as the EPA's Photochemical Assessment Monitoring Stations network. The Ad-Hoc Ceilometer Evaluation Study (ACES) was designed to help guide the implementation of hourly MLHs for the EPA's PAMS network through the evaluation of commercial ceilometer signal, firmware, software, and the development of a unified PBL retrieval algorithm. Data from four commercial ceilometers (Lufft CHM15k, Vaisala CL51, Vaisala

CL31, and Campbell SkyVUE PRO) deployed during ACES were used to develop and assess the application of the proposed common algorithm.

Instrument signal quality is first addressed by implementing signal corrections for known and documented noise, artifacts, and overlap issues in aerosol backscatter profiles measured by commercially available instrumentation. The algorithm then uses continuation and time-tracking parameters to aid in layer attribution and reduce misidentification of aerosol layers during transition times. The retrieval method also derives cloud-base heights using wavelet method, routinely screens for precipitation, and calculates uncertainties in the PBLH retrieval. The algorithm is tested against radiosonde PBLHs and CBHs. A total of 58 radiosonde profiles were used and retrievals were attributed to diurnal layers of the PBL evolution (i.e., nocturnal stable layer, residual layer, and mixing layer). The goal of these retrievals is for the reliable and automated retrieval of PBL layers for the use of the scientific community including climatological, meteorological, air quality, dispersion, and numerical model evaluation.

Overall good agreement was found for all comparisons, with no statistically significant bias found except for the cases of SL comparisons and daytime ML using SkyVUE PRO ceilometer measurements. It can be concluded that nighttime shallow SL retrievals should not be used without auxiliary measurements for verification and minimum height limitations, and SkyVUE

PRO retrievals should take extra care to account for signal artifacts and quality. Nighttime retrievals of RL heights revealed overall good correlations with radiosonde RL heights (squared correlation coefficients r^2 ranging from 0.89 to 0.96 and bias from ~ -131 to $+63$ m). However, a reduced output for RLs was reported by all comparisons because nighttime hours typically contain various aerosol layering and therefore can introduce more uncertainty in nighttime retrievals. Daytime ML heights showed the best agreement with radiosonde heights (r^2 ranging from 0.88 to 0.97 and bias from -119 to $+101.07$ m).

The comparison also revealed significant limitations when using the SkyVUE PRO ceilometer as it displayed the lowest correlations, overall overestimation of PBLHs, and the highest bias. While during daytime 44% of retrievals were excluded, 55% of retrievals were excluded during nighttime indicating that more than half of SkyVUE PRO profiles were unreliable for PBL detection using the method detailed in this study.

A novel approach of the proposed algorithm was the estimation of uncertainties of retrievals. Using the calculated standard deviation of individual PBLH retrievals to further quality assess retrievals, all comparisons remain with bias below 200 m. Although this final algorithm constraint reduces final retrievals (6%–55% removal of retrievals), it increased correlations to radiosonde heights for all comparisons in this study.

With minimal changes in the overlap design, calibrations, firmware, and therefore signal quality in commercial ceilometers expected, the proposed algorithm only requires modifications to $Z_{\max}$ and the input for local sunset and sunrise times with each instrument location. Although results show overall good agreement, it should be noted that additional limitations can arise in varying environments. For instance, Caicedo et al. (2019) found that coastal circulations and multiple layering (e.g., internal boundary layers) can lead to errors in PBLH detection. Similarly, mountainous regions typically experience stratification associated with complex topography and airmass flows (Smith et al. 2002; De Wekker et al. 2004). These occasional yet not uncommon complex environments can increase both aerosol stratification and algorithm uncertainties therefore limiting the proposed retrieval algorithm. Future work with a larger dataset will help determine the extent of these limitations under various meteorological conditions and environments.

Although this study uses a challenging dataset collected during the winter season, good agreement was found compared to radiosonde PBLH. Improved agreement is anticipated for warmer, convective, and greater aerosol loading time periods were stratification is reduced and well-mixed PBLs are expected. As this work shows, the automated precipitation and cloud screening, continuation constraints, and uncertainty limitations result in reliable PBL retrievals. Future work should address the standardization of ceilometer measurements as heterogeneous networks become operational along with noise removal tools with focus on the CL31 and SkyVUE PRO ceilometers.

The research described in this article has been reviewed by the U.S. Environmental Protection Agency (EPA) and approved for publication. Approval does not signify that the contents necessarily reflect the views and the policies of the agency nor does mention of trade names or commercial products constitute endorsement or recommendation for use.

Data availability statement. Ceilometer and radiosonde data used in this study are available online (https://alg.umbc.edu/ACES).

REFERENCES

Baars, H., A. Ansmann, R. Engelmann, and D. Althausen, 2008: Continuous monitoring of the boundary-layer top with lidar. *Atmos. Chem. Phys.*, **8**, 7281–7296, https://doi.org/10.5194/acp-8-7281-2008.

——, and Coauthors, 2016: An overview of the first decade of PollyNET: An emerging network of automated Raman-polarization lidars for continuous aerosol profiling. *Atmos. Chem. Phys.*, **16**, 5111–5137, https://doi.org/10.5194/acp-16-5111-2016.

Biavati, G., D. G. Feist, C. Gerbig, and R. Kretschmer, 2015: Error estimation for localized signal properties: Application to atmospheric mixing height retrievals. *Atmos. Meas. Tech.*, **8**, 4215–4230, https://doi.org/10.5194/amt-8-4215-2015.

Bonin, T. A., B. J. Carroll, R. M. Hardesty, W. A. Brewer, K. Hajny, O. E. Salmon, and P. B. Shepson, 2018: Doppler lidar observations of the mixing height in Indianapolis using an automated composite fuzzy logic approach. *J. Atmos. Oceanic Technol.*, **35**, 473–490, https://doi.org/10.1175/JTECH-D-17-0159.1.

Bradley, R. S., F. T. Keimig, and H. F. Diaz, 1993: Recent changes in the North American Arctic boundary layer in winter. *J. Geophys. Res.*, **98**, 8851–8858, https://doi.org/10.1029/93JD00311.

Brooks, I. M., 2003: Finding boundary layer top: Application of a wavelet covariance transform to lidar backscatter profiles. *J. Atmos. Oceanic Technol.*, **20**, 1092–1105, https://doi.org/10.1175/1520-0426(2003)020<1092:FBLTAO>2.0.CO;2.

Caicedo, V., B. Rappenglück, B. Lefer, G. Morris, D. Toledo, and R. Delgado, 2017: Comparison of aerosol lidar retrieval methods for boundary layer height detection using ceilometer aerosol backscatter data. *Atmos. Meas. Tech.*, **10**, 1609–1622, https://doi.org/10.5194/amt-10-1609-2017.

——, and Coauthors, 2019: Bay breeze and sea breeze circulation impacts on the planetary boundary layer and air quality from an observed and modeled DISCOVER-AQ Texas case study. *J. Geophys. Res. Atmos.*, **124**, 7359–7378, https://doi.org/10.1029/2019JD030523.

Cohn, S., and W. Angevine, 2000: Boundary layer height and entrainment zone thickness measured by lidars and wind-profiling

radars. *J. Appl. Meteor.*, **39**, 1233–1247, https://doi.org/10.1175/1520-0450(2000)039<1233:BLHAEZ>2.0.CO;2.

Compton, J. C., R. Delgado, T. A. Berkoff, and R. M. Hoff, 2013: Determination of planetary boundary layer height on short spatial and temporal scales: A demonstration of the covariance wavelet transform in ground-based wind profiler and lidar measurements. *J. Atmos. Oceanic Technol.*, **30**, 1566–1575, https://doi.org/10.1175/JTECH-D-12-00116.1.

Dang, R., Y. Yang, X.-M. Hu, Z. Wang, and S. Zhang, 2019: A review of techniques for diagnosing the atmospheric boundary layer height (ABLH) using aerosol lidar data. *Remote Sens.*, **11**, 1590, https://doi.org/10.3390/rs11131590.

Davis, K. J., N. Gamage, C. R. Hagelberg, C. Kiemle, D. H. Lenschow, and P. P. Sullivan, 2000: An objective method for deriving atmospheric structure from airborne lidar observations. *J. Atmos. Oceanic Technol.*, **17**, 1455–1468, https://doi.org/10.1175/1520-0426(2000)017<1455:AOMFDA>2.0.CO;2.

de Bruine, M., A. Apituley, D. Donovan, H. Klein Baltink, and M. de Haij, 2017: Pathfinder: Applying graph theory for consistent tracking of daytime mixed layer height with backscatter lidar. *Atmos. Meas. Tech.*, **10**, 1893–1909, https://doi.org/10.5194/amt-10-1893-2017.

de Haij, M., W. Wauben, and H. Klein Baltink, 2006: Determination of mixing layer height from ceilometer backscatter profiles. *Proc. SPIE*, **6362**, 63620R, https://doi.org/10.1117/12.691050.

Delle Monache, L., K. D. Perry, R. T. Cederwall, and J. A. Ogren, 2004: In situ aerosol profiles over the Southern Great Plains and cloud and radiation test bed site: 2. Effects of mixing height on aerosol properties. *J. Geophys. Res.*, **109**, D06209, https://doi.org/10.1029/2003JD004024.

De Wekker, S. F. J., D. G. Steyn, and S. Nyeki, 2004: A comparison of aerosol-layer and convective boundary-layer structure over a mountain range during STAAARTE '97. *Bound.-Layer Meteor.*, **113**, 249–271, https://doi.org/10.1023/B:BOUN.0000039371.41823.37.

Di Giuseppe, F., A. Riccio, L. Caporaso, G. Bonafé, G. P. Gobbi, and F. Angelini, 2012: Automatic detection of atmospheric boundary layer height using ceilometer backscatter data assisted by a boundary layer model. *Quart. J. Roy. Meteor. Soc.*, **138**, 649–663, https://doi.org/10.1002/qj.964.

Emeis, S., K. Schäfer, and C. Münkel, 2008a: Long-term observations of the urban mixing-layer height with ceilometers. *IOP Conf. Ser. Earth Environ. Sci.*, **1**, 012027, https://doi.org/10.1088/1755-1315/1/1/012027.

——, ——, and ——, 2008b: Surface-based remote sensing of the mixing-layer height—A review. *Meteor. Z.*, **17**, 621–630, https://doi.org/10.1127/0941-2948/2008/0312.

EPA, 2019: Technical assistance document for sampling and analysis of ozone precursors for the Photochemical Assessment Monitoring Stations program—Revision 2—April 2019. EPA Doc. EPA-454/B-19-004, 226 pp.

Eresmaa, N., A. Karppinen, S. M. Joffre, J. Räsänen, and H. Talvitie, 2006: Mixing height determination by ceilometer. *Atmos. Chem. Phys.*, **6**, 1485–1493, https://doi.org/10.5194/acp-6-1485-2006.

Garratt, J. R., 1992: *The Atmospheric Boundary Layer*. Cambridge University Press, 335 pp.

Geiß, A., 2016: Automated calibration of ceilometer data and its applicability for quantitative aerosol monitoring. Ph.D. thesis, Ludwig-Maximilians-Universität München, 185 pp.

——, and Coauthors, 2017: Mixing layer height as an indicator for urban air quality? *Atmos. Meas. Tech.*, **10**, 2969–2988, https://doi.org/10.5194/amt-10-2969-2017.

Haeffelin, M., and Coauthors, 2012: Evaluation of mixing-height retrievals from automatic profiling lidars and ceilometers in view of future integrated networks in Europe. *Bound.-Layer Meteor.*, **143**, 49–75, https://doi.org/10.1007/s10546-011-9643-z.

Haman, C. L., B. Lefer, and G. A. Morris, 2012: Seasonal variability in the diurnal evolution of the boundary layer in a near-coastal urban environment. *J. Atmos. Oceanic Technol.*, **29**, 697–710, https://doi.org/10.1175/JTECH-D-11-00114.1.

——, E. Couzo, J. H. Flynn, W. Vizuete, B. Heffron, and B. L. Lefer, 2014: Relationship between boundary layer heights and growth rates with ground-level ozone in Houston, Texas. *J. Geophys. Res. Atmos.*, **119**, 6230–6245, https://doi.org/10.1002/2013JD020473.

Heffter, J. L., 1980: Transport layer depth calculations. *Second Joint Conf. on Applications of Air Pollution Meteorology*, New Orleans, LA, Amer. Meteor. Soc., 787–791.

Hervo, M., Y. Poltera, and A. Haefele, 2016: An empirical method to correct for temperature-dependent variations in the overlap function of CHM15k ceilometers. *Atmos. Meas. Tech.*, **9**, 2947–2959, https://doi.org/10.5194/amt-9-2947-2016.

Hicks, M., R. Sakai, and E. Joseph, 2015: The evaluation of a new method to detect mixing layer heights using lidar observations. *J. Atmos. Oceanic Technol.*, **32**, 2041–2051, https://doi.org/10.1175/JTECH-D-14-00103.1.

——, B. Demoz, K. Vermeesch, and D. Atkinson, 2019: Intercomparison of mixing layer heights from the National Weather Service ceilometer test sites and collocated radiosondes. *J. Atmos. Oceanic Technol.*, **36**, 129–137, https://doi.org/10.1175/JTECH-D-18-0058.1.

Holzworth, G. C., 1964: Estimates of mean maximum mixing depths in the contiguous United States. *Mon. Wea. Rev.*, **92**, 235–242, https://doi.org/10.1175/1520-0493(1964)092<0235:EOMMMD>2.3.CO;2.

Hopkin, E., A. J. Illingworth, C. Charlton-Perez, C. D. Westbrook, and S. Ballard, 2019: A robust automated technique for operational calibration of ceilometers using the integrated backscatter from totally attenuating liquid clouds. *Atmos. Meas. Tech.*, **12**, 4131–4147, https://doi.org/10.5194/amt-12-4131-2019.

Knepp, T. N., and Coauthors, 2017: Assessment of mixed-layer height estimation from single-wavelength ceilometer profiles. *Atmos. Meas. Tech.*, **10**, 3963–3983, https://doi.org/10.5194/amt-10-3963-2017.

Kotthaus, S., and C. S. B. Grimmond, 2018a: Atmospheric boundary layer characteristics from ceilometer measurements. Part 1: A new method to track mixed layer height and classify clouds. *Quart. J. Roy. Meteor. Soc.*, **144**, 1525–1538, https://doi.org/10.1002/qj.3299.

——, and ——, 2018b: Atmospheric boundary layer characteristics from ceilometer measurements. Part 2: Application to London's urban boundary layer. *Quart. J. Roy. Meteor. Soc.*, **144**, 1511–1524, https://doi.org/10.1002/qj.3298.

——, E. O'Connor, C. Münkel, C. Charlton-Perez, M. Haeffelin, A. M. Gabey, and C. S. B. Grimmond, 2016: Recommendations for processing atmospheric attenuated backscatter profiles from Vaisala CL31 ceilometers. *Atmos. Meas. Tech.*, **9**, 3769–3791, https://doi.org/10.5194/amt-9-3769-2016.

Lammert, A., and J. Bösenberg, 2006: Determination of the convective boundary-layer height with laser remote sensing. *Bound.-Layer Meteor.*, **119**, 159–170, https://doi.org/10.1007/s10546-005-9020-x.

Lewis, J. R., E. J. Welton, A. M. Molod, and E. Joseph, 2013: Improved boundary layer depth retrievals from MPLNET.

J. Geophys. Res. Atmos., **118**, 9870–9879, https://doi.org/10.1002/JGRD.50570.

Liu, S., and X.-Z. Liang, 2010: Observed diurnal cycle climatology of planetary boundary layer height. *J. Climate*, **23**, 5790–5809, https://doi.org/10.1175/2010JCLI3552.1.

Lotteraner, C., and M. Piringer, 2016: Mixing-height time series from operational ceilometer aerosol-layer heights. *Bound.-Layer Meteor.*, **161**, 265–287, https://doi.org/10.1007/s10546-016-0169-2.

Madonna, F., F. Amato, J. Vande Hey, and G. Pappalardo, 2015: Ceilometer aerosol profiling versus Raman lidar in the frame of the INTERACT campaign of ACTRIS. *Atmos. Meas. Tech.*, **8**, 2207–2223, https://doi.org/10.5194/amt-8-2207-2015.

——, and Coauthors, 2018: Intercomparison of aerosol measurements performed with multiwavelength Raman lidars, automatic lidars and ceilometers in the framework of INTERACT-II campaign. *Atmos. Meas. Tech.*, **11**, 2459–2475, https://doi.org/10.5194/amt-11-2459-2018.

Marsik, F. J., K. W. Fischer, T. D. McDonald, and P. J. Samson, 1995: Comparison of methods for estimating mixing height used during the 1992 Atlanta field intensive. *J. Appl. Meteor.*, **34**, 1802–1814, https://doi.org/10.1175/1520-0450(1995)034<1802:COMFEM>2.0.CO;2.

Martucci, G., R. Matthey, V. Mitev, and H. Richner, 2007: Comparison between backscatter lidar and radiosonde measurements of the diurnal and nocturnal stratification in the lower troposphere. *J. Atmos. Oceanic Technol.*, **24**, 1231–1244, https://doi.org/10.1175/JTECH2036.1.

——, ——, ——, and ——, 2010: Frequency of boundary-layer-top fluctuations in convective and stable conditions using laser remote sensing. *Bound.-Layer Meteor.*, **135**, 313–331, https://doi.org/10.1007/s10546-010-9474-3.

Mather, P., 1987: *Computer Processing of Remotely-Sensed Images*. John Wiley and Sons, 353 pp.

McElroy, J. L., and T. B. Smith, 1991: Lidar descriptions of mixing-layer thickness characteristics in a complex terrain/coastal environment. *J. Appl. Meteor.*, **30**, 585–597, https://doi.org/10.1175/1520-0450(1991)030<0585:LDOMLT>2.0.CO;2.

Morille, Y., M. Haeffelin, P. Drobinski, and J. Pelon, 2007: STRAT: An automated algorithm to retrieve the vertical structure of the atmosphere from single-channel lidar data. *J. Atmos. Oceanic Technol.*, **24**, 761–775, https://doi.org/10.1175/JTECH2008.1.

Münkel, C., and R. Roininen, 2010: Automatic monitoring of boundary layer structures with ceilometers. *Vaisala News*, No. 184, 7–9, https://www.vaisala.com/sites/default/files/documents/vn184_07_AutomaticMonitoringofBoundaryLayerStructureswithCeilometers.pdf.

——, N. Eresmaa, J. Räsänen, and A. Karppinen, 2007: Retrieval of mixing height and dust concentration with lidar ceilometer. *Bound.-Layer Meteor.*, **124**, 117–128, https://doi.org/10.1007/s10546-006-9103-3.

O'Connor, E. J., A. J. Illingworth, and R. J. Hogan, 2004: A technique for autocalibration of cloud lidar. *J. Atmos. Oceanic Technol.*, **21**, 777–786, https://doi.org/10.1175/1520-0426(2004)021<0777:ATFAOC>2.0.CO;2.

Pal, S., M. Haeffelin, and E. Batchvarova, 2013: Exploring a geophysical process based attribution technique for the determination of the atmospheric boundary layer depth using aerosol lidar and near-surface meteorological measurements. *J. Geophys. Res. Atmos.*, **118**, 9277–9295, https://doi.org/10.1002/JGRD.50710.

Peng, J., and Coauthors, 2017: Ceilometer based analysis of Shanghai's boundary layer height (under rain and fog free conditions). *J. Atmos. Oceanic Technol.*, **34**, 749–764, https://doi.org/10.1175/JTECH-D-16-0132.1.

Piringer, M., K. Baumann, and M. Langer, 1998: Summertime mixing heights at Vienna, Austria, estimated from vertical soundings and by a numerical model. *Bound.-Layer Meteor.*, **89**, 25–45, https://doi.org/10.1023/A:1001565319487.

Poltera, Y., G. Martucci, M. Collaud Coen, M. Hervo, L. Emmenegger, S. Henne, D. Brunner, and A. Haefele, 2017: PathfinderTURB: An automatic boundary layer algorithm. Development, validation and application to study the impact on in situ measurements at the Jungfraujoch. *Atmos. Chem. Phys.*, **17**, 10 051–10 070, https://doi.org/10.5194/acp-17-10051-2017.

Rappenglück, B., R. Perna, S. Zhong, and G. A. Morris, 2008: An analysis of the vertical structure of the atmosphere and the upper-level meteorology and their impact on surface ozone levels in Houston, Texas. *J. Geophys. Res.*, **113**, D17315, https://doi.org/10.1029/2007JD009745.

Scarino, A. J., and Coauthors, 2014: Comparison of mixed layer heights from airborne high spectral resolution lidar, ground-based measurements, and the WRFChem model during CalNex and CARES. *Atmos. Chem. Phys.*, **14**, 5547–5560, https://doi.org/10.5194/acp-14-5547-2014.

Schäfer, K., S. M. Emeis, A. Rauch, C. Munkel, and S. Vogt, 2004: Determination of mixing layer heights from ceilometer data. *Proc. SPIE*, **5571**, 248–259, https://doi.org/10.1117/12.565592.

Seibert, P., F. Beyrich, S. E. Gryning, S. Joffre, A. Rasmussen, and P. Tercier, 2000: Review and intercomparison of operational methods for the determination of the mixing height. *Atmos. Environ.*, **34**, 1001–1027, https://doi.org/10.1016/S1352-2310(99)00349-0.

Seidel, D. J., C. O. Ao, and K. Li, 2010: Estimating climatological planetary boundary layer heights from radiosonde observations: Comparison of methods and uncertainty analysis. *J. Geophys. Res.*, **115**, D16113, https://doi.org/10.1029/2009JD013680.

——, Y. Zhang, A. Beljaars, J.-C. Golaz, A. R. Jacobson, and B. Medeiros, 2012: Climatology of the planetary boundary layer over the continental United States and Europe. *J. Geophys. Res.*, **117**, D17106, https://doi.org/10.1029/2012JD018143.

Sivaraman, C., S. McFarlane, E. Chapman, M. Jensen, T. Toto, S. Liu, and M. Fischer, 2013: Planetary boundary layer (PBL) height value added product (VAP): Radiosonde retrievals. U.S. Department of Energy Rep. DOE/SC-ARM-TR-132, 36 pp., https://www.arm.gov/publications/tech_reports/doe-sc-arm-tr-132.pdf.

Smith, R. B., S. T. Skubis, J. D. Doyle, A. Broad, C. Kiemle, and H. Volkert, 2002: Mountain waves over Mont Blanc: Influence of a stagnant boundary layer. *J. Atmos. Sci.*, **59**, 2073–2092, https://doi.org/10.1175/1520-0469(2002)059<2073:MWOMBI>2.0.CO;2.

Snyder, B. J., and K. B. Strawbridge, 2004: Meteorological analysis of the Pacific 2001 Air Quality Field Study. *Atmos. Environ.*, **38**, 5733–5743, https://doi.org/10.1016/j.atmosenv.2004.02.068.

Sokół, P., I. S. Stachlewska, I. Ungureanu, and S. Stefan, 2014: Evaluation of the boundary layer morning transition using the CL-31 ceilometer signals. *Acta Geophys.*, **62**, 367–380, https://doi.org/10.2478/s11600-013-0158-5.

Sørensen, J. H., A. Rasmussen, T. Ellermann, and E. Lyck, 1998: Mesoscale influence on long-range transport, evidence from ETEX modelling and observations. *Atmos. Environ.*, **32**, 4207–4217, https://doi.org/10.1016/S1352-2310(98)00183-6.

Steyn, D. G., M. Baldi, and R. M. Hoff, 1999: The detection of mixed layer depth and entrainment zone thickness from

lidar backscatter profiles. *J. Atmos. Oceanic Technol.*, **16**, 953–959, https://doi.org/10.1175/1520-0426(1999)016<0953:TDOMLD>2.0.CO;2.

Stull, R. B., 1988: *An Introduction to Boundary Layer Meteorology*. Kluwer Academic, 666 pp.

Tang, G., and Coauthors, 2016: Mixing layer height and its implications for air pollution over Beijing, China. *Atmos. Chem. Phys.*, **16**, 2459–2475, https://doi.org/10.5194/acp-16-2459-2016.

Toledo, D., C. Córdoba-Jabonero, and M. Gil-Ojeda, 2014: Cluster analysis: A new approach applied to lidar measurements for atmospheric boundary layer height estimation. *J. Atmos. Oceanic Technol.*, **31**, 422–436, https://doi.org/10.1175/JTECH-D-12-00253.1.

Troen, I., and L. Mahrt, 1986: A simple model of the atmospheric boundary layer; sensitivity to surface evaporation. *Bound.-Layer Meteor.*, **37**, 129–148, https://doi.org/10.1007/BF00122760.

Uzan, L., S. Egert, and P. Alpert, 2016: Ceilometer evaluation of the eastern Mediterranean summer boundary layer height—First study of two Israeli sites. *Atmos. Meas. Tech.*, **9**, 4387–4398, https://doi.org/10.5194/amt-9-4387-2016.

Vande Hey, J., J. Coupland, J. Richards, and A. Sandford, 2012: Design and implementation of a divided lens lidar ceilometer prototype for manufacture. *IEEE Int. Geoscience and Remote Sensing Symp.*, Munich, Germany, IEEE, 5002–5005, https://doi.org/10.1109/IGARSS.2012.6352488.

van der Kamp, D., and I. McKendry, 2010: Diurnal and seasonal trends in convective mixed-layer heights estimated from two years of continuous ceilometer observations in Vancouver, BC. *Bound.-Layer Meteor.*, **137**, 459–475, https://doi.org/10.1007/s10546-010-9535-7.

Wagner, P., and K. Schäfer, 2017: Influence of mixing layer height on air pollutant concentrations in an urban street canyon. *Urban Climate*, **22**, 64–79, https://doi.org/10.1016/j.uclim.2015.11.001.

Wang, Z., X. Cao, L. Zhang, J. Notholt, B. Zhou, R. Liu, and B. Zhang, 2012: Lidar measurement of planetary boundary layer height and comparison with microwave profiling radiometer observation. *Atmos. Meas. Tech.*, **5**, 1965–1972, https://doi.org/10.5194/amt-5-1965-2012.

Wiegner, M., and A. Geiß, 2012: Aerosol profiling with the Jenoptik ceilometer CHM15kx. *Atmos. Meas. Tech.*, **5**, 1953–1964, https://doi.org/10.5194/amt-5-1953-2012.

——, and Coauthors, 2019: Aerosol backscatter profiles from ceilometers: Validation of water vapor correction in the framework of CeiLinEx2015. *Atmos. Meas. Tech.*, **12**, 471–490, https://doi.org/10.5194/amt-12-471-2019.

Zhang, J., H. Chen, Z. Li, X. Fan, L. Peng, Y. Yu, and M. Cribb, 2010: Analysis of cloud layer structure in Shouxian, China using RS92 radiosonde aided by 95 GHz cloud radar. *J. Geophys. Res.*, **115**, D00K30, https://doi.org/10.1029/2010JD014030.